Combustion of Hydrocarbon Fuels at Normal and Elevated Pressures

Research Paper for the Austrian Marshall Plan Foundation

Ao.Univ.Prof. Dipl.-Ing. Dr.techn. Ernst Pucher
E 315 - Institut für Fahrzeugantriebe und Automobiltechnik
Technische Universität Wien

Prof. Dr. Kalyanasundaram Seshadri
Department of Mechanical and Aerospace Engineering
University of California, San Diego, USA

By:

Mathias Innerkofler
Matrikel Nr.: 1028051
Wachtelweg 17
A-9400 Wolfsberg

Wien, June 2018

Abstract

Experimental and computational investigations are carried out to elucidate the influences of the amount of fuel and oxygen on critical conditions of autoignition and extinction of n-heptane, n-decane, and n-dodecane in laminar non-premixed flows. These conditions depend on the characteristic flow time and the characteristic chemical time. The characteristic flow time is given by the strain rate. The chemical time depends on the adiabatic flame temperature and the stoichiometric mixture fraction. The experiments are carried out employing the counterflow configuration. In this configuration, two streams flow toward a stagnation plane. One stream called the fuel-stream is made up of vaporized fuel and nitrogen, and the other stream called the oxidizer-stream is made up of oxygen and nitrogen. The experiments were conducted at a pressure of 1.13 atm. The parameters that influence autoignition are mass of the fuel stream $Y_{F,1}$, temperature of the fuel stream, T_1, mass fraction of oxygen in the oxidizer stream, $Y_{O_2,2}$, temperature of the oxidizer stream, T_2, and strain rate a_2. Computations were performed using detailed chemistry and the predictions are compared with measurements.

Table of Contents

1. Introduction

Today's modern society is closely linked to the automobile. The need for the automobile is also reflected in the 600 million cars that are on the road worldwide. The majority of these cars are powered by conventional internal combustion engines, which are reciprocating piston engines with internal combustion. These internal combustion engines represent one of the most efficient heat engines on the market. Internal combustion engines are not only used in commercial vehicles, but also in shipping and as generators in power engineering, where depending on the drive concept efficiencies of over 50 percent can be achieved. Latest forecasts show that the number of vehicles will almost double by the middle of the century, from 600 million to about 1.1 billion vehicles. However, this also results in a steadily growing social and political pressure on the automotive industry in terms of pollutant emissions, recyclability and fuel consumption of newly developed vehicles. The main focus will be on reducing pollutant emissions and CO_2 emissions. The CO_2 emissions released by the combustion of fossil fuels are greenhouse gases and thus jointly responsible for global warming. Road traffic also contributes to global warming and pollution, albeit to a limited extent. Combustion of a modern gasoline engine with a 3-way catalytic converter produces about 72.5% N_2, about 13.5% CO_2, 12.5% H_2O and 0.8% O_2 and other inert gases. Less than 1% of the exhaust gases are considered harmful and legally limited. Nevertheless, the majority of the population is concerned about the environmental impact of the automobile, as well as its resources and energy consumption. Conventional combustion engines will continue to dominate as a drive concept in vehicles over the next few decades due to their flexibility, compactness and efficiency. The European Commission has predicted that by 2030, up to 40 percent of all kilometers traveled will be in metropolitan areas. For this purpose, it is necessary to understand the fundamental processes occurring during combustion and to further reduce the resulting pollutants in order to both allow the cleanest possible road traffic, and to continue to ensure an urban habitat in metropolitan areas. The research of the subsequent master thesis is addressing the problems of combustion phenomena, such as autoignition and extinction by employing a counter flow configuration. The thesis involves a theoretical part on combustion physics and chemical kinetics as well as an experimental section on structures of hydrocarbon diffusion flames of prevaporized n-

heptane, n-decane and n-dodecane, including experimental measurements and numerical computations with full chemical-kinetic mechanisms.

2. Principle of the Atmospheric Pressure Counterflow Burner

The two basic categories of flame propagation are the premixed and non-premixed propagation. In premixed flames the fuel and the oxidizer are mixed prior the reaction zone. The stoichiometry of the mixture can be controlled by changing the fuel to oxidized ratio, and an inert gas such as nitrogen is used to dilute the reactants and vary the flame temperature. An example where a premixed flame propagation takes place is the combustion chamber of common used gasoline engines. In gasoline engines, the fuel and oxidizer are mixed before they are injected into the cylinder. Diffusion flames or also called non-premixed flames occur when the fuel and oxidizer are not mixed prior to reacting. The oxidizer is supplied from the ambient air and the mixing and combustion reactions take place together [1]. Counterflow diffusion flames in general are very often used experimentally because they are better controllable and stable compared to non-premixed flames and they also represent a one-dimension diffusion flame structure. In Diesel engines for example, the fuel is injected into the cylinder near the top dead center. During the so-called ignition delay time, the fuel atomizes into droplets, vaporizes and the mixing with air occurs simultaneously until the temperature in the cylinder reaches the fuel ignition temperature [1] [2].

In the present thesis, all experiments are carried out with a non-premixed laminar counterflow setup. The critical conditions of autoignition and extinction are measured employing an atmospheric pressure counterflow burner. This counterflow burner consists of two axisymmetric ducts opposing each other. The lower duct is called the fuel duct, as a mixture of vaporized fuel and nitrogen enters the reaction zone. The upper duct is called the oxidizer duct and guides the oxidizer, which consists of a mixture of pure nitrogen and oxygen, into the reaction zone. Both streams are assumed to be steady, laminar and axisymmetric. A stagnation plane is generated by impinging the uniform oxidizer stream against the uniform fuel stream. In the near of the stagnation plane a thin viscous boundary layer establishes. Due to manually ignition or an autoignition event a flame occurs and stabilizes in the thin viscose layer in the

vicinity of this surface if the local mixture fraction gradient is sufficiently high [3]. The combustion in a counter flow burner is mainly dependent on the chemical reaction time, and the flow velocities of the fuel and the oxidizer.
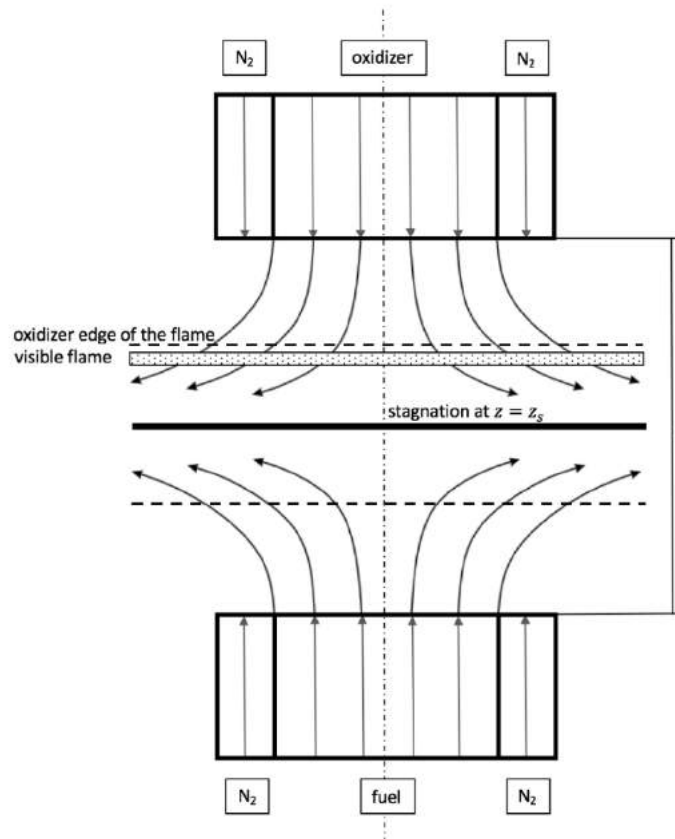

Figure 1: Schematic illustration of a counterflow flame generated by opposing nozzles. The structure of the flame consists of a reaction zone which separates a fuel rich zone and an oxidizer rich zone.

During the experiments with counter flow diffusion flames, the following three additional desirable characteristics are presumed [4]:

- The tangential components of the flow velocities at the boundaries are zero and the flow velocities along the centerline near the stagnation plane varies linearly with distance. These favorable characteristics allow to constitute the flow with the local strain rate a. The value of the strain rate is defined as the normal gradient of the normal component of the flow velocity. A detailed description and derivation of the strain rate will be exercised chapter 2.4.2.

- The symmetry of the counterflow flame leads to planar or well-defined curvatures

- The inverse of the velocity gradient represents the characteristic flow time. By comparing the characteristic flow time to the characteristic reaction time, the Damköhler number is revealed,

$$Da = \frac{Reaction\ rate}{Diffusion\ rate} = \frac{Diffusion\ time}{Reaction\ time} \ .$$

In order to stabilize the flame and also to shield the reactants from the environment, curtains or also called guard flows are used. These guard flows consist of nitrogen or other inert gases and have no influence on the reaction zone. During the experiments with the counterflow burner the product gases are sucked downward into the lower part of the burner and are cooled down using water sprays which are adjusted inside the lower burner body. Furthermore, the water sprays also prevent potential flame propagation through the exhaust system.

2.1. Strain Rate

In counterflow configurations the strain rate is a useful tool to characterize the flow field and to quantify the velocities of the flows. A mathematical concept for deriving the strain rate in counterflow flames was developed by Seshadri, et al. [3] [5]. The strain rate is defined as the normal gradient of the normal component of the flow velocity. The strain rate at the oxidizer stream is different to the strain rate at the fuel stream. The strain rate a_2 at the oxidizer stream is given by

$$a_2 = \frac{2|V_2|}{L}\left(1 + \frac{|V_1|\sqrt{\rho_1}}{|V_2|\sqrt{\rho_2}}\right)$$

with ρ1 as the density of the fuel stream at the boundary [kg/m3] and respectively ρ2 as the density of the oxidizer stream at the boundary [kg/m3]. L stands for the distance [m] between the fuel duct and the oxidizer duct. V1 and V2 denote the normal components of the flow velocities [m/s] for the fuel duct and for the oxidizer duct, respectively. The equation is developed from an asymptotic theory where the Reynolds

numbers of the laminar flows at the duct exits are assumed to be large. The Equation of the strainrate is then reduced to the following simplification.

$$V_2 = \frac{a_2 L}{4}$$

According to this equation the velocity of the oxidizer stream can be calculated with a given oxidizer strain rate.

2.2. Critical States of Ignition and Extinction

In combustion applications, irregular combustion processes play a very important role in terms of both efficiency and pollutant formation. In gasoline engines for example the knocking combustion is an irregular combustion process. To achieve high partial load efficiency today's modern gasoline engines, have a very high compression ratio. This can lead to thermodynamically critical conditions in the combustion chamber in the full load range, which subsequently lead to a self-autoignition event of the fuel-air mixture. In contrast to the normal combustion the so-called knocking combustion in the still unburned mixture occurs at the end of the compression process at one or more locations on a self-ignition event. As a result, the knocking combustion leads to strong pressure fluctuations in the combustion chamber which are reflected at the combustion chamber walls and lead to an increase in emissions of pollutants [2]. The second critical combustion performance factor in combustion applications is the state of extinction. The main source of unburned HC emissions in a gasoline engine is the incomplete flame spread due to extinction of the flame on the cold cylinder walls [2]. In general, low emission engines use techniques such as advanced fuel-air mixing strategies, exhaust gas recirculation and staged injection, which can be affected by flame extinction. Flame extinction is characterized by the operating conditions, local fuel/air ratio and the reaction chemistry of the fuel. [1] [2]

In computational models the causes of these two critical states can be determined with the Damköhler number for extinction Da_{ext} and for autoignition Da_{ign}.

3. Materials and Methods

Experimental studies are carried out to characterize the critical conditions of the autoignition and extinction event of three different pure hydrocarbon fuels by employing the counterflow configuration setup. Figure 2 shows a schematic illustration of the setup. The tested liquid fuels are vaporized by using a vaporizer. The flow rates of gases are adjusted by computer-regulated mass flow controllers. All flow lines between the vaporizer and the fuel duct were heated up by a heating tape to prevent condensation of fuel inside the piping and the vaporizer. A process controller controls the heating tape. The temperatures of the vaporizer exit and injection, as well as the fuel duct and the oxidizer temperature are measured with adjusted thermocouples. The flow rates of the used gases are adjusted by computer-regulated mass flow controllers. The various components are discussed in the following chapters.
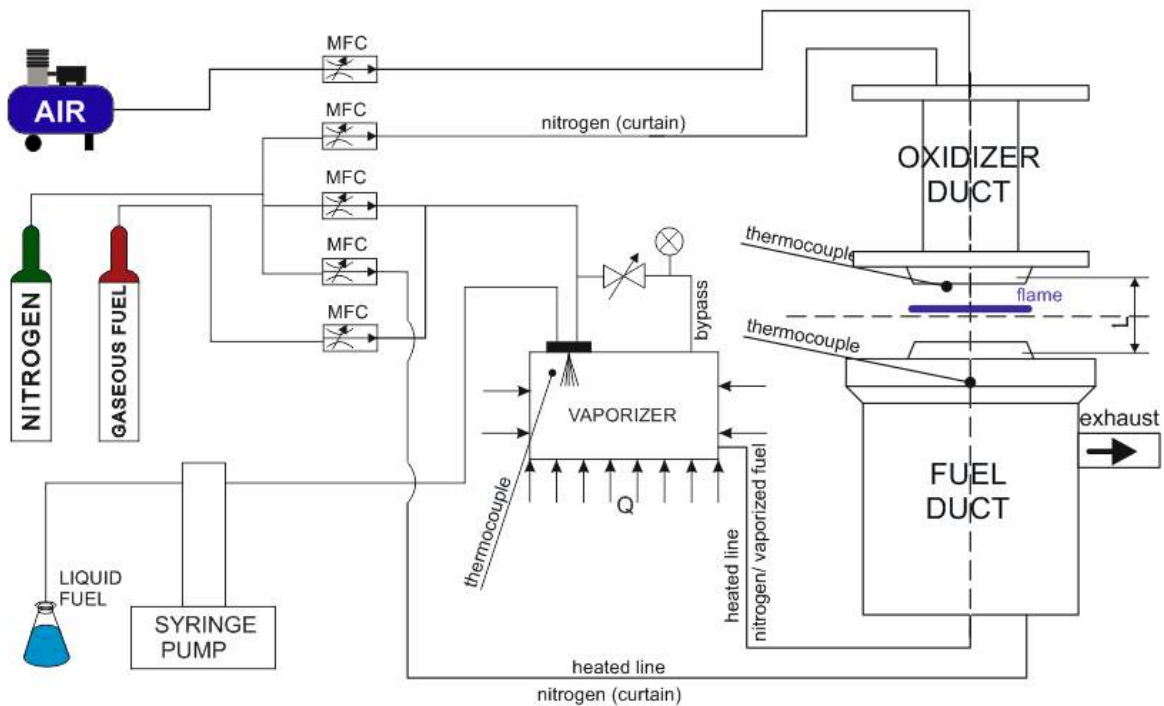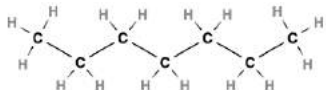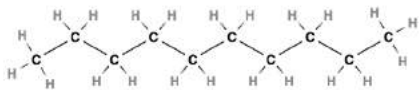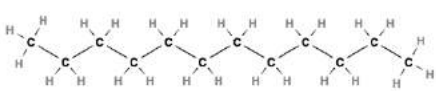

Figure 2: Schematic illustration of the experimental setup, consisting of the counterflow burner, gas and fuel supply and the mass flow controllers

3.1. Tested Fuels

Hydrocarbons consist of only carbon and hydrogen atoms and are one of the most significant classes of organic compounds. A large part of most common used fossil fuels and jet fuels consists of hydrocarbons, in particular hydrocarbons that contain between 6 and 10 carbon atoms [1]. In this thesis the combustion behavior of Alkanes, in particular n-heptane, n–decane and n–dodecane is analyzed. These pure fuels are referred to as saturated straight chain hydrocarbons and are the simplest class of their type. Saturated hydrocarbons in general consist of hydrogen and carbon atoms which are linked together with only single bonds and every carbon atom is bonded to as many hydrogen atoms as possible. The properties of the three different tested fuels can be found in Table 1.

Table 1: Properties of n-heptane, n-decane and n-dodecane [6] [7] [8]

fuel	chemical formula	molar mass [g/mol]	density at 300 K [kg/m^3]	boiling point [K]
n-heptane	C_7H_{16}	100.2019	678.03	371.53
n-decane	$C_{10}H_{22}$	142.2817	725.09	447.27
n-dodecane	$C_{12}H_{26}$	170.3348	744.36	489.3

- n-heptane

n-heptane is a colorless liquid with a gasoline like odor and it is the major component in common used gasoline fuels. Due to its short chain length and molecular structure it burns explosively, and it sets along with pure octane the extreme ends of the octane rating scale.

- n-decane

n-decane is a colorless liquid with 22 hydrogen atoms and 10 carbon atoms. The higher number on carbon atoms lead to a higher boiling point and to a higher molecular weight compared to n-heptane. This liquid pure fuel is used in experimental studies to develop and investigate surrogates for jet fuels.

- n-dodecane

n-dodecane has the highest molecular weight of all three tested fuels and it is an oily clear liquid fuel of the paraffin series. Due to its molecular structure, it is also used as a compound in surrogates for jet fuels and in surrogates for diesel fuels.

3.2. Lower Part of the Burner

The lower part of the burner is a complex aluminum construction with the aim to guide the gaseous fuel stream into the reaction zone and to cool down the exhaust gases with water spray nozzles to prevent further reactions. The fuel stream is guided through the main duct into the reaction zone. At the end of this fuel duct three stainless screens are adjusted each separated by a stainless-steel ring. A thermocouple is adjusted in front of the screens on the inlet side to measure the fuel stream temperature before entering the reaction zone. The curtain duct surrounds the fuel duct and creates co-flow jets of Nitrogen, which stabilize the fuel and also the oxidizer stream in the reaction zone at the borders and prevent any chemical reactions with ambient air. The exhaust gases are sucked away from the reaction zone by vacuum into the internal building extraction system.

3.3. Upper Part of the Burner

The upper part of the burner or also called oxidizer duct is the most essential part of the experimental setup. It guides the oxidizer stream into the reaction zone and it also produces steady, laminar plug flow conditions which are the key points in the

counterflow theory. Each top is connected to the lower part of the burner via three adjustable pins for setting the separation distance L.

The extinction top consists of a main duct and a surrounding annular curtain duct. The main duct guides the oxidizer stream into the reaction zone and steady laminar flow conditions with axially directed exit velocities are formed by 3 stainless steel screens at the end of the duct. All screens are held in place by 5 steel rings. These fine woven screens from Inconel have a high resistance to high temperatures and to corrosive environments. The curtain duct with a honeycomb ring close to the end of the duct to ensure plug flow conditions guides the nitrogen curtains surround the flame to stabilize it and to shield the reactants from the environment. The composition of the autoignition top is similar to that of the extinction top. Key part of the autoignition top is a Starbar®SER silicon carbide heating element with a central heating section referred to as a hot zone and two terminal sections called cold ends to heat up the oxidizer stream to the autoignition temperature. Temperatures of up to $1300\,K$ degrees can be achieved with this powerful heating element. The heating element is surrounded by a quartz oxidizer duct and an annular quartz curtain duct. To prevent any damage or melting of all the non-ceramic parts the autoignition top is provided with a water cooling system. Furthermore, the curtain duct isolated with high-temperature Insulfrax® S Blankets. The screens used at the autoignition top are the same screens used at the extinction top and the fuel duct.

3.4. Vaporizer

During the experiments at the atmospheric counterflow burner only liquid fuels were investigated. Both for autoignition as well as for extinction experiments the fuels needed to be vaporized. Therefore, a vaporizer which simplified consists of a heated aluminium box, a BETE fog XA SR 050 fuel injection nozzle, a Bete FC07 fluid cap and a Bete AC1201 air cap is used.

The vaporizern is also inisolated with high-temperature Insulfrax® S Blankets used at the autoignition top. Vaporized fuel in the vaporizer is prevented from being ignited and burnt therein by various manners, such as leakproofness, controlling an air/fuel ratio in a range out of a combustible range and keeping vaporized fuel temperature at a level lower than its self-igniting temperature. Nitrogen is used for dilution and to carry the vaporized fuel to the burner. The temperature inside the vaporizer as well as inside

the lines running from the vaporizer to the reactions zone is controlled by heating tapes and process controllers to prevent re-condensation of the vaporized fuel. The fuel injection nozzle uses the energy in compressed gas to produce highly atomized sprays at low flow rates. The nozzle is cooled by a cooling plate attached to the bottom to avoid vaporization which would influence the constant flow. The liquid fuel is supplied to the nozzle under pressure from a Teledyne Hastings 500D Syringe pump with flowrates between 0 ml/min and 15 l/min

3.5. LabView Controlling Software

To obtain most accurate and reproducible results, the entire experimental setup is controlled and monitored with a visual programming language from National Instruments, called LabVIEW. The self-developed control software uses a dataflow programming language and has been constantly improved and further developed over the years. One benefit of this software is the simple monitoring, controlling and adaptation of hardware such as mass flow controllers, pumps and calibration devices. For the experiments on the atmospheric counterflow burner up to 5 gaseous reactants as well as one liquid reactant in each stream can be controlled. Figure 3 shows the basic control front panel of the VI during an autoignition event. The basic control front panel allows the operator to input data such as oxidizer strain rate (in the upper left), mass fractions of the fuel stream, oxidizer stream as well as of the curtains (lower right). Furthermore, this front panel allows to control the different flowrates of the streams as well as of the temperatures of the fuel stream and oxidizer stream.
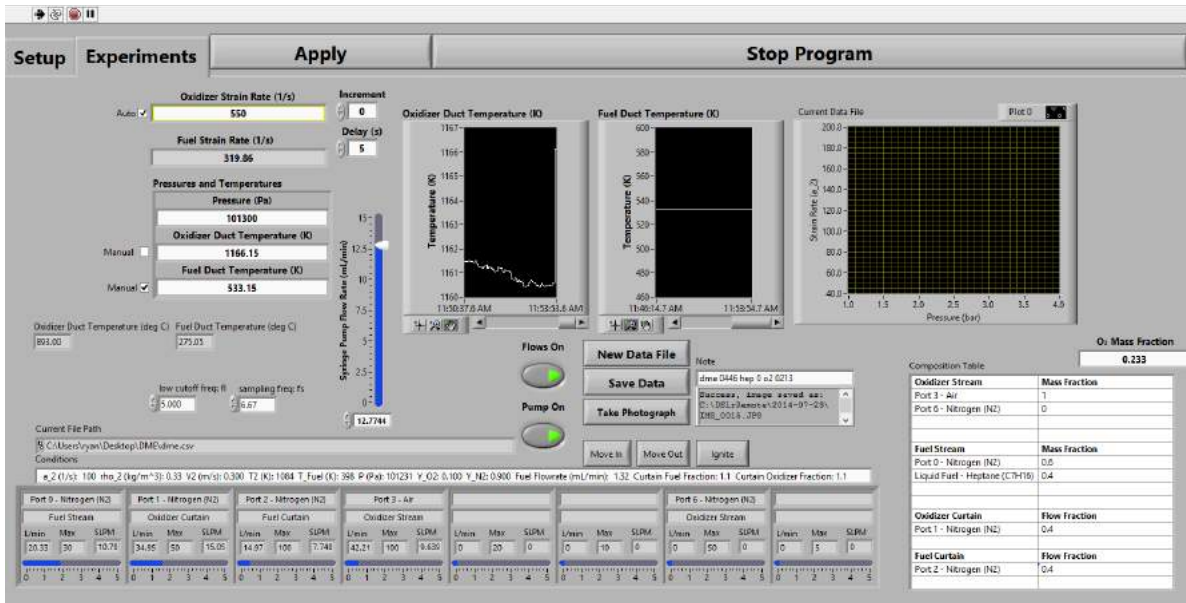
Figure 3: Basic control front panel of the counterflow software during an autoignition event

The main front panel for the software is shown in Figure 4. Before carrying out an experiment it is necessary to set up all the ports and reactant streams depending on the needed maximum flowrates as well as the type of the experiment.
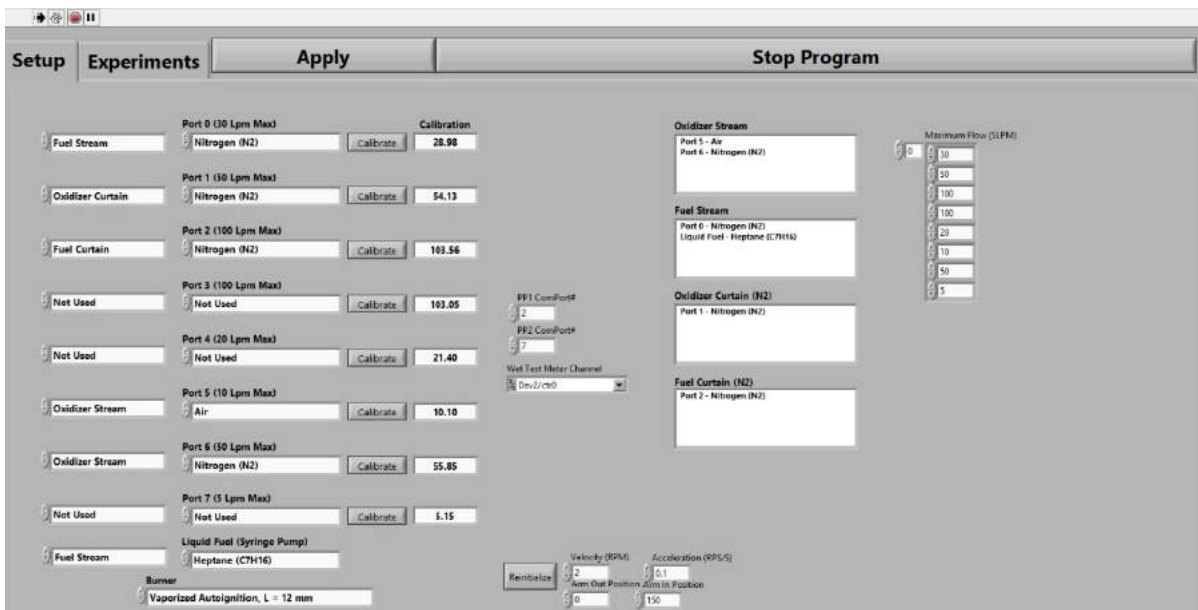

Figure 4: main front panel of the counterflow software

3.1. Gas Flow Control and Calibration

A mass flow controller is a device that automatically establishes and controls a stable flow rate of liquids or gases according to a set flow rate sent as an electric signal linear to the mass flow rate. During the experiments with the counter flow burner several Teledyne mass flow controllers are used. The controllers have flow ranges from 0-50 slm to flows of 0-100 slm and a full-scale accuracy of about 1 %. In order to obtain very accurate result, the mass flow controllers must be calibrated for the maximum flow rate in the respective working range for each individual gas needed. For the calibration of the mass flow controller a volumetric RITTER Drum-type Gas Meter with a flow range of 0.167 l/min to 33.3 l/min and a National Instruments USB-6008 device are used. The measurement device meter works on the principle of displacement and contains a revolving measuring drum within a packing liquid. The gas flowing through the meter causes a rotation of the measuring drum within the packaging fluid and the volume gets measured by periodically filling and emptying the four rigid measuring chambers. The USB device counts the pulses corresponding to the turns of the measuring drum in order to determine the volumetric flow rate. This type of gas meter is used because of the direct measurement of volumes which means that the conditions and compositions of gases have no influence on the measurement accuracy. Before each calibration, the level of the packing liquid must be checked carefully to ensure an accurate calibration. After the port of the mass flow controller is physically connected to the measurement device the calibration can be controlled using a Labview calibration routine. During the calibration the value of the maximum volumetric flowrate is directly measured, and an updated calibration value is calculated. The calibration procedure is repeated until the accuracy of the deviation of the mass flow controllers is less than $\pm 1\%$ and the standard deviation is less than $\pm 0.01\%$. Figure 5 shows the front panel of the calibration VI during the calibration procedure where the deviation of the mass flow controllers is less than $\pm 1\%$ and the standard deviation is less than $\pm 0.01\%$.
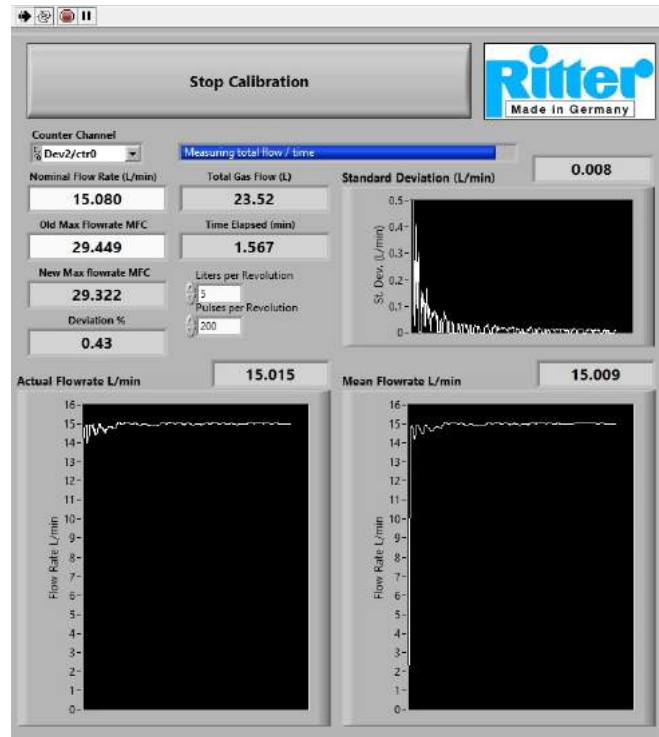
Figure 5: Front panel of the calibration VI during the calibration procedure where the deviation of the mass flow controllers is less than $\pm 1\%$ and the standard deviation is less than $\pm 0.01\%$.

3.2. Temperature Measurement and Control

Thermocouples are used for experimental diagnostics in combustion research and in high temperature processes where a quantitative knowledge of the gas temperature is required to determine appropriate kinetic rate constants and to calculate heat fluxes associated with high temperature flows. When carrying out counterflow experiments, it is necessary to know and to control the gas temperatures in the system. Especially in the pre-vaporization of a liquid fuel in the vaporizer it is important to set and control the temperatures in order to ensure complete vaporization of the liquid fuel and to prevent filling the vaporizer with the liquid fuel. After the fuel is getting vaporized it is also necessary to set the temperatures of the lines between the vaporizer and the burner high enough to prevent condensation of the fuel. Furthermore, the temperature of the vaporized fuel at the fuel boundary must be known for proper control of flow rates such that the gases are injected with a known temperature and velocity for later use in numerical codes. A proper and exact feedback of the fuel ducts is necessary to control the temperature using a PID-loop process controller and also for providing real-time temperature feedback to the Labview control software. The temperatures of the fuel stream are measured with two E-type thermocouples. These two thermocouples

are placed beneath the screens on the fuel duct side. One thermocouple is connected with an Omega CN4416 temperature/process controller to control heating tapes along the flow lines. The second thermocouple is used for the so-called cold junction compensation. Therefore, the thermocouple is connected with a USB-TC module which can be used by the Labview software. Two additional E-type thermocouples are used to measure the temperatures at the vaporizor inlet and vaporizer outlet. During the autoignition experiments on the atmospheric counterflow burner a Pt/13%Rh-Pt R-type thermocouple is used to measure the oxidizer stream temperature at the oxidizer exit. This type of a thermocouple is used because of high service temperatures and stabilities. [9]

3.3. Experimental Procedure

- Autoignition at Atmospheric Pressure

The critical conditions of autoignition are measured at an ambient pressure level of $1.013\ bar$ with prevaporized liquid fuels diluted with nitrogen and an oxidizer stream consisting of oxygen and nitrogen. The temperature of the oxidizer stream at autoignition as a function of the fuel mass fraction $Y_{F,1}$ at fixed values of $Y_{O_2,2} = 0.233$, and strain rate $a_2 = 550s^{-1}$ as well as the temperature of the oxidizer stream at autoignition as a function of the mass fraction of oxygen $Y_{O_2,2}$ at fixed values of $Y_{F,1} = 0.4$, and strain rate $a_2 = 550s^{-1}$ are investigated. For each individual experiment the density at $300\ K$ and the molecular weight of each fuel is entered into the VI. In order to obtain accurate results, the mass flow controllers are calibrated for the maximum flow rate in the respective working range for each individual gas before every experimentation. For every single fuel, both the experiments with fixed fuel mass fractions and various oxidizer mass fractions as well as the experiments with fixed oxidizer mass fractions and various fuel mass fractions are carried out in one day to make sure that during the experiments the same ambient conditions apply. After the calibration of the mass flow controllers the separation distance between the two ducts is set to $12\ mm$, the cooling system is turned on and the vaporizer and the flow lines are heated up to the defined temperature. During the heating of the vaporizer and the flowlines a constant fuel stream flow of only nitrogen prevents local overheating's of

the system. The thermocouple is then adjusted as close as possible to the screens at the end of the oxidizer duct to measure the oxidizer stream temperature at autoignition. The screens at the autoignition top are replaced after every experimentation or if any warping or damage was visible. After that the syringe pump is flushed and filled with the fuel being examined. Before heating up the autoignition top a low arbitrary strain rate is set and a flame is established with a blowtorch to control the shape of the flame and the ignitability of the mixture. The flame is held for 10 to 20 seconds to ensure that there are no residues of other fuels in the system. After that the autoignition top is heated up very slowly to avoid any thermal stress and damage. During the heating of the autoignition top a constant low oxidizer flow stream, consisting of nitrogen and oxygen, ensures an overheating of the top and it also avoids a pure nitrogen atmosphere around the Starbar heating element. Especially at high temperatures a pure nitrogen atmosphere can result in a formation of an insulative silicon nitride layer around the heating element and to an over-temperature damage. Before reaching an estimated autoignition temperature the separation distance is checked and adjusted again because of the high heat strain of the ceramic oxidizer duct. When approaching the expected autoignition temperature all streams used are set to their defined values and the experiment can start. To investigate the oxidizer stream temperature at a certain point it is necessary to hold the temperature of the oxidizer stream at that point as constant as possible. Then the fuel pump is turned on. It is very important to maintain the fuel stream for at least 20 seconds to ensure good mixing of the reactants inside the reaction zone. If no autoignition event occurs the fuel pump is turned off and the temperature of the oxidizer stream is increased about $5 \ [K]$. Then the procedure is repeated again until an autoignition event shown in Figure 3 occurs. After the first autoignition event occurs the oxidizer stream temperature is then decreased in steps of about $1 \ [K]$. Every single step is examined for auto-ignition. The last point where a self-ignition of the mixture occurs is recorded and this point is examined at least 5 times.
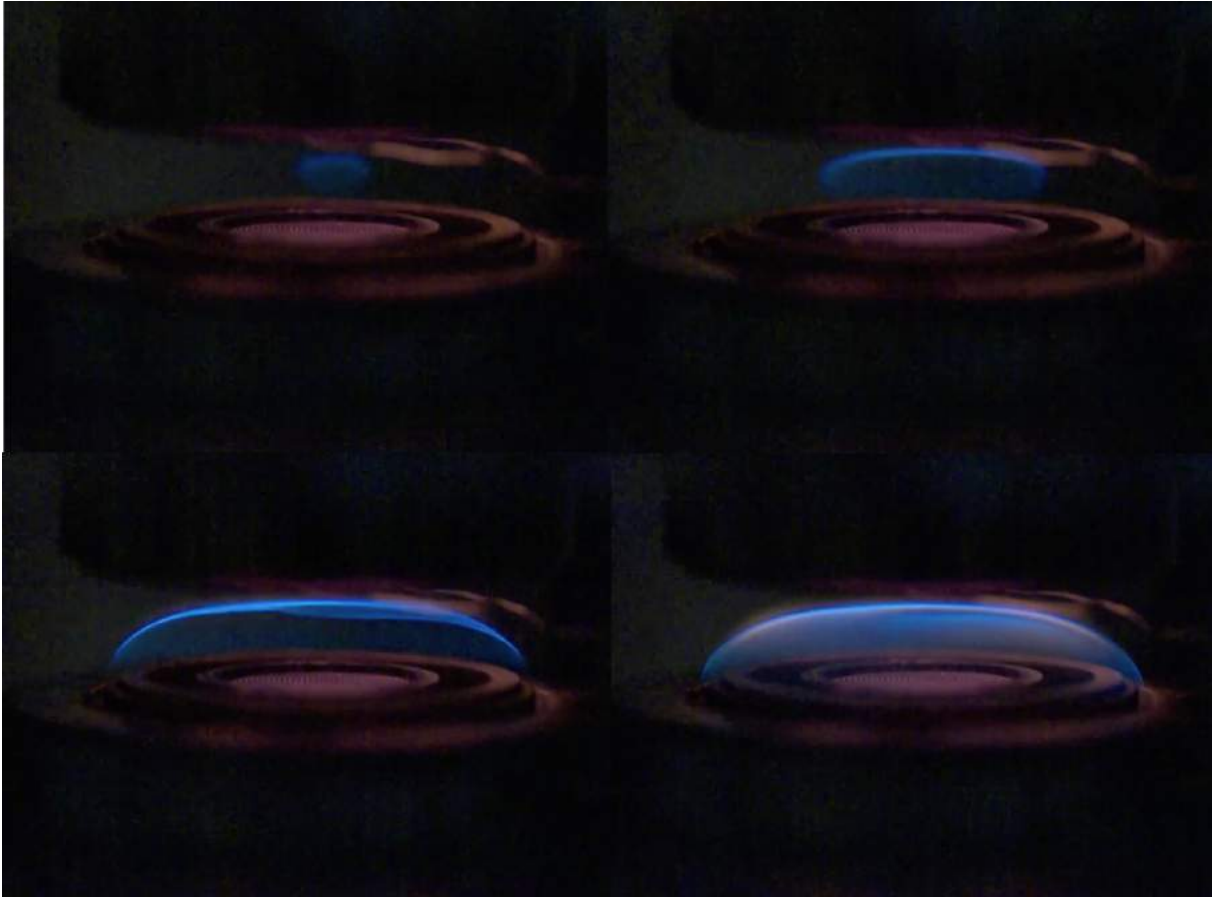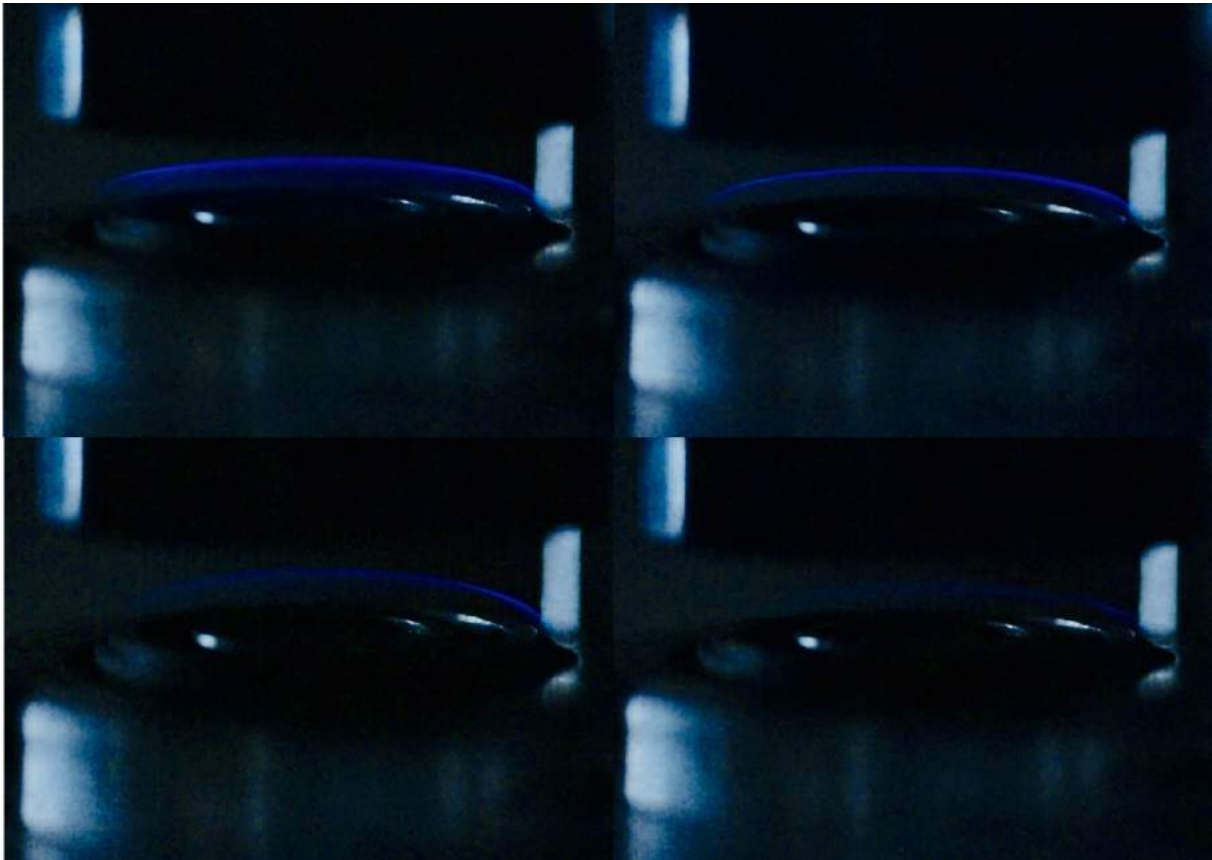
Figure 6: High speed image of an autoignition event with heptane with a fuel mass fraction of $Y_{F,1} = 0.4$, oxidizer strain rate $a_2 = 550\ s^{-1}$ and pure air as an oxidizer.

- Extinction at Atmospheric Pressure

The critical conditions of extinction are measured at an ambient pressure level of $1.013\ bar$ with prevaporized liquid fuels and with fixed values of $Y_{O_2,2} = 0.233$ and various values of $Y_{F,1}$. Before starting the extinction experiments the separation distance between the two ducts is set to 10 mm and also the VI is set to the extinction setup. As same as in the autoignition experiments the cooling system is turned on and the vaporizer and the flowlines are heated up to a defined temperature and the pump is flushed and filled with the fuel being examined. During the heating of the vaporizer and the flowlines a constant fuel stream flow of only nitrogen prevents local overheating's of the system. After the defined temperatures are reached a control flame is established with a blowtorch and held for 10 to 20 seconds. To investigate a specific point, an arbitrary strain rate below the expected extinction strain rate is set and a flame is established with a blow torch. Then the oxidizer strain rate is increased at a relatively high rate of $10s^{-1}$ every 5 seconds in order to obtain a rough assessment

where the flame will extinguish. As soon as the flame extinguishes a new strain rate below the first extinction strain rate is set, a new flame is established, and the oxidizer strain rate is than increased at a rate of $5s^{-1}$ every 5 seconds. The strainrate where the flame extinguishes for the second time is saved and the mass flow controllers are calibrated for this flow rate in this working range for every individual gas used in the experiment. After that a strain rate close to the extinction strain rate is set and a flame is established. The strain rate is then increased with a rate of $1s^{-1}$ every 8 seconds until the flame extinguishes. This procedure is repeated at least five times for every point to be examined to obtain results as accurate as possible.

Figure 7: High speed image of an extinction event with heptane with a fuel mass fraction of $Y_{F,1} = 0.3$, oxidizer strain rate $a_2 = 345\ s^{-1}$ and pure air as an oxidizer.

4. Discussion of the Experimental- and Numerical Results of the Atmospheric Pressure Counterflow Burner

Chapter 4 summarizes and compares both the experimental and numerical results. The detailed results of the extinction and the autoignition experiments are attached in the appendix.

4.1. Results of the Autoignition Experiments

The autoignition experiments were carried out with prevaporized n-heptane, n-decane and n-dodecane at different fuel stream temperatures to investigate the influence of different fuel- and oxygen mass fractions on the autoignition event. The experiments with different fuel mass fractions were conducted from the lowest fuel mass fraction of $Y_{F,1} = 0.25$ to the highest fuel mass fraction of $Y_{F,1} = 0.5$. The experiments with different oxygen mass fractions were conducted from the lowest oxygen mass fraction of $Y_{O_2,2} = 0.07$ to the highest oxygen mass fraction of $Y_{O_2,2} = 0.233$. The displayed experimental data points are arithmetically averaged values and all results are corrected due to radiation losses.

Figure 8 shows the temperature of the oxidizer stream at autoignition, $T_{2,ign}$ as a function of the mass fraction of oxygen $Y_{O_2,2}$ for n-heptane and n-decane. The figure depicts that the autoignition temperature increases with reducing the oxygen mass fraction. Furthermore, the autoignition characteristics of n-heptane and n-decane are similar. Due to the higher number of carbon atoms of-n-decane, the auto-ignition temperature is lower compared to n-heptane. In other words, heavier hydrocarbons tend to auto-ignite before lighter hydrocarbons. The difference in the autoignition temperature between both fuels at an oxygen mass fraction $Y_{O_2,2} = 0.233$ is $17.51\ [K]$. The difference in the autoignition temperature between both fuels at an oxygen mass fraction $Y_{O_2,2} = 0.07$ is $17.17\ [K]$.
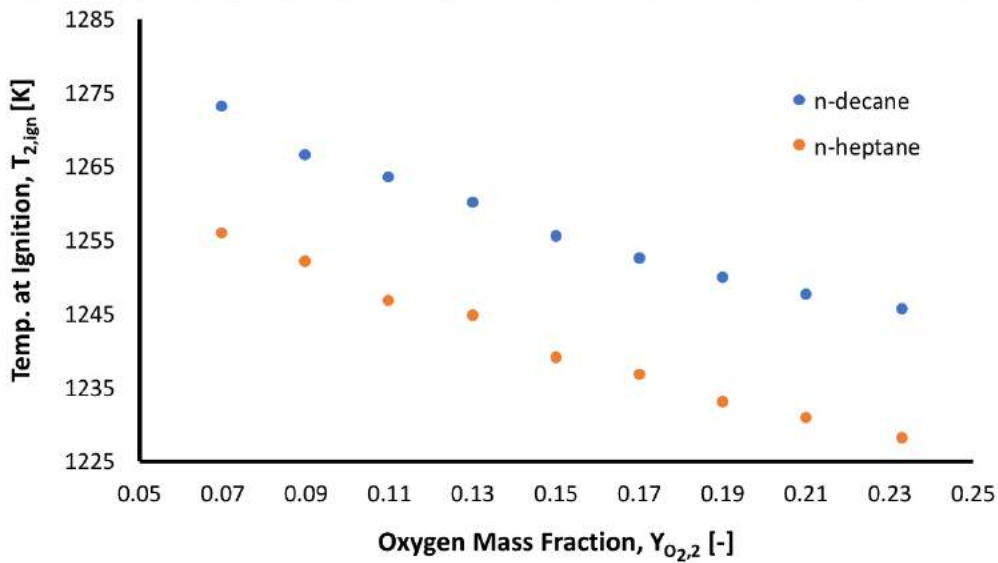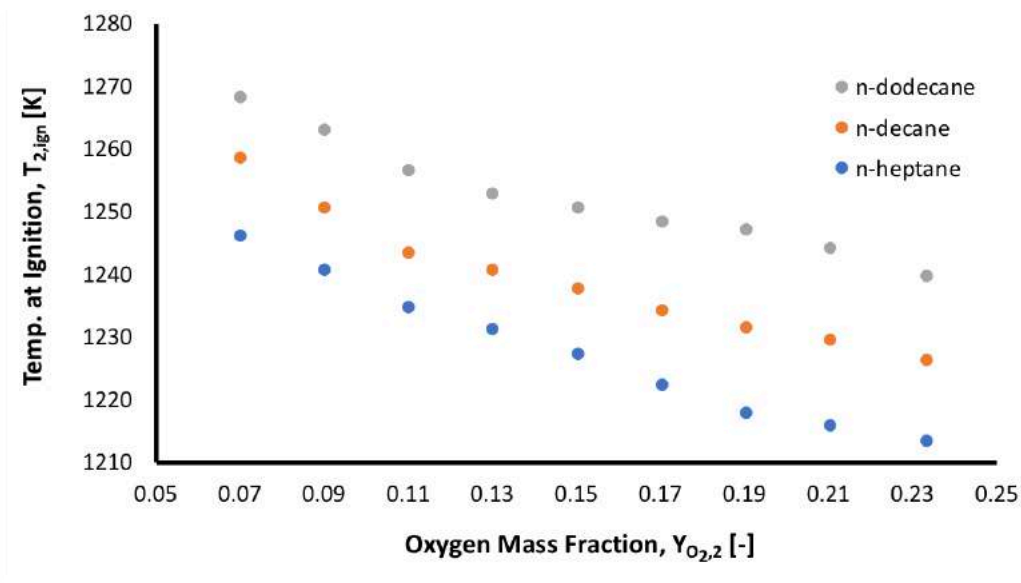
Figure 8: The temperature of the oxidizer stream at autoignition, $T_{2,ign}$ as a function of the mass fraction of oxygen $Y_{O_2,2}$ for $Y_{F,1} = 0.4$, $T_1 = 473\ [K]$ and $a_2 = 550\ s^{-1}$.
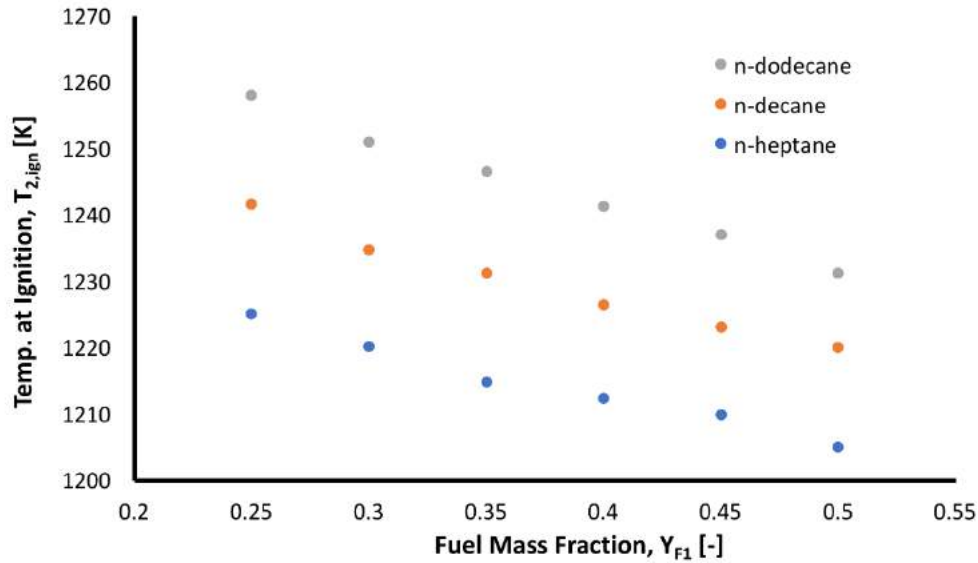
Figure 9 illustrates the temperature of the oxidizer stream at autoignition, $T_{2,ign}$, as a function of the mass fraction of fuel $Y_{F,1}$ for n-heptane and n-decane. The results show that a variation of the fuel ass fraction has a greater influence on the autoignition temperature compared to a variation of the oxygen mass fraction. However, both experiments show a similar characteristic.
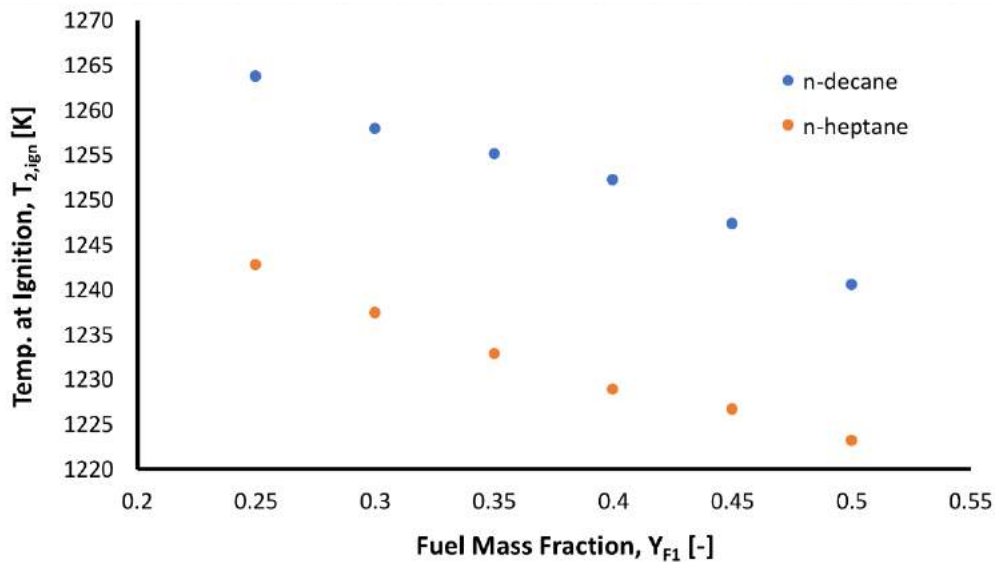
Figure 9: The temperature of the oxidizer stream at autoignition, $T_{2,ign}$ as a function of the mass fraction of fuel $Y_{F,1}$ for $Y_{O_2,2} = 0.233$, $T_1 = 473\ [K]$ and $a_2 = 550\ s^{-1}$.

The experimental autoignition limits of the second set of experiments are illustrated in Figure 10 and Figure 11. In these experiments a fuel stream temperature $T_1 = 533.15 \ [K]$ was used. The higher temperature was set because of the higher boiling point of n-dodecane, to prevent condensation of fuel inside the piping and the vaporizer. When comparing n-heptane, n-decane and n-dodecane all results show a similar characteristic. Do-decane is found to have the highest autoigniton temperatures due to the highest number of carbon atoms of all tested fuels. Furthermore, the results of n-heptane and n-decane at a fuel stream temperature of $T_1 = 533.15 \ [K]$ show a lower autoignition temperature when compared to the results in Figure 8 and Figure 9. It can be assumed that also n-dodecane shows this trend at a fuel stream temperature of $T_1 = 473.15 \ [K]$. Even at higher fuel stream temperatures a variation of the fuel mass fraction has a greater influence on the autoignition temperature compared to a variation of the oxygen mass fraction.
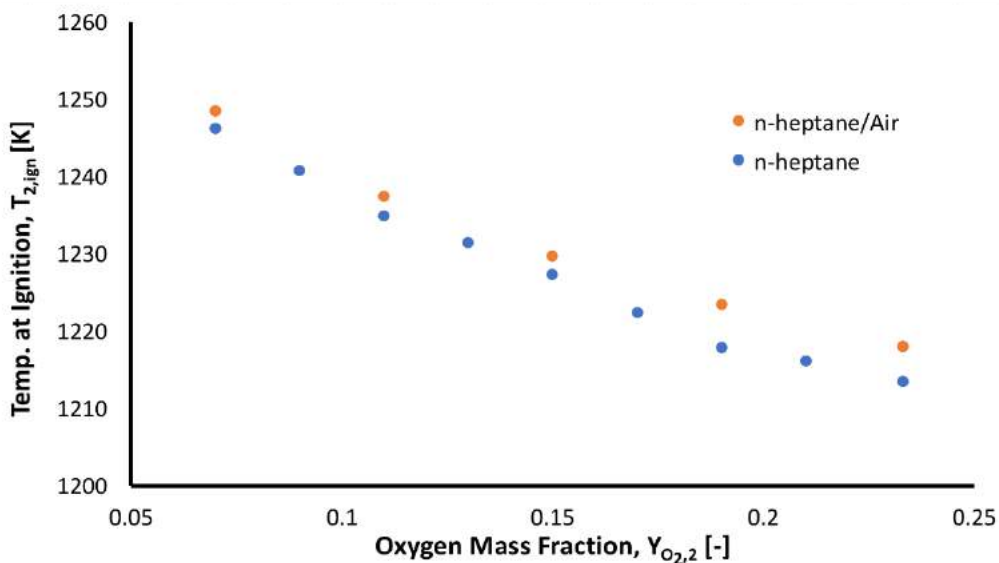

Figure 10: The temperature of the oxidizer stream at autoignition, $T_{2,ign}$ as a function of the mass fraction of oxygen $Y_{O_2,2}$ for $Y_{F,1} = 0.4$, $T_1 = 533.15 \ [K]$ and $a_2 = 550 \ s^{-1}$.

Figure 11: The temperature of the oxidizer stream at autoignition, $T_{2,ign}$ as a function of the mass fraction of fuel $Y_{F,1}$ for $Y_{O_2,2} = 0.233$, $T_1 = 533.15\ [K]$ and $a_2 = 550\ s^{-1}$.

The kinematic models for the extinction experiments were carried out with OpenSMOKE++ using a detailed chemical-kinematic mechanism made up of more than 13,000 elementary and lumped reactions among more than 352 species. At the fuel-boundary and oxidizer-boundary, the temperatures, T_1 and T_2 and the injection speeds of the fuel-stream v_1, oxidizer-stream v_2, are prescribed. For the numerical simulations plug flow conditions were used to describe the flow field and both Soret effect and gas radiation were included in the simulations. In Figure 12 and Figure 14 the numerically calculated values of the critical conditions of autoignition of n-heptane, n-decane and n-dodecane are compared with the data obtained during the experiments. The lines represent boundaries separating a region above where autoignition takes place from a region below where autoignition cannot take place.

Figure 12 shows the temperature of the oxidizer stream at autoignition as a function of the oxygen mass fractions for all tested fuels. The obtained experimental data points illustrate that the autoignition temperature increases with reducing the oxygen mass fraction. Whereas the numerical calculated values of the critical conditions of autoignition for n-heptane, n-decane, and n-dodecane show a completely different characteristic. The calculated values of critical conditions of autoignition show that the oxygen mass fraction in the oxidizer stream has no influence on the autoignition temperature and the results represent almost horizontal lines over the examined area. Hence, it was of great interest to ensure that the experimental setup was correct and

that no errors occurred during the experiment, especially during the mixing of the oxidizer consisting of N_2 and O_2. Therefore, a third experiment with n-heptane was carried out using clean compressed air as an oxidizer. The result of this experiment is illustrated in Figure 13. The figure shows that even with pure air as an oxidizer, the trend is still the same. The little difference in the autoignition temperature between the experiments using pure air and self-mixed air as an oxidizer is assumed to be related to a new adjustment of the thermocouple.
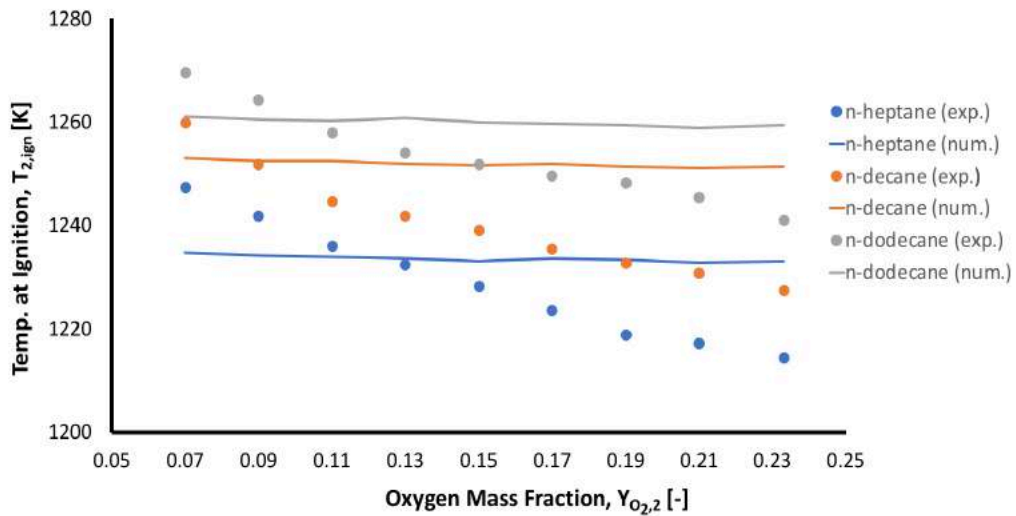
Figure 12: Comparison of the numerical calculations with the experimental results of the temperature of the oxidizer stream at autoignition $T_{2,ign}$ as a function of the mass fraction of oxygen $Y_{O_2,2}$ for $Y_{F,1} = 0.4$, $T_1 = 533.15\ [K]$ and $a_2 = 550\ s^{-1}$.

Figure 13: The temperature of the oxidizer stream at autoignition, $T_{2,ign}$ as a function of the mass fraction of oxygen $Y_{O_2,2}$ for $Y_{F,1} = 0.4$, $T_1 = 533.15\ [K]$ and $a_2 = 550\ s^{-1}$.

Figure 14 shows the temperature of the oxidizer stream at autoignition as a function of the fuel mass fractions for n-heptane, n-decane and n-dodecan. The numerically calculated values of the critical conditions of autoignition agree well with experimental data. The experimental data and the calculated values of critical conditions of autoignition show that n-heptane is easiest to ignite followed by n-decane and n-dodecane. Even though the numerical data over predicts the absolute values obtained by the experimental work at all fuel mass fractions, the computational data shows the same characteristic.
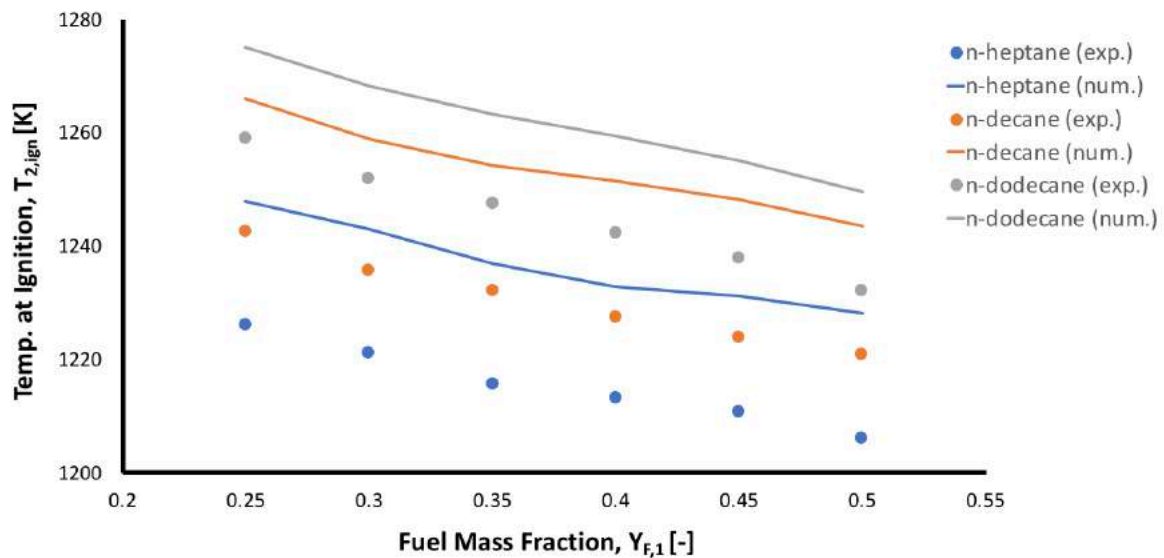
Figure 14: Comparison of the numerical calculations with the experimental results of the temperature of the oxidizer stream at autoignition $T_{2,ign}$ as a function of the mass fraction of fuel $Y_{F,1}$ for $Y_{O_2,2} = 0.233$, $T_1 = 533.15\,[K]$ and $a_2 = 550\,s^{-1}$.
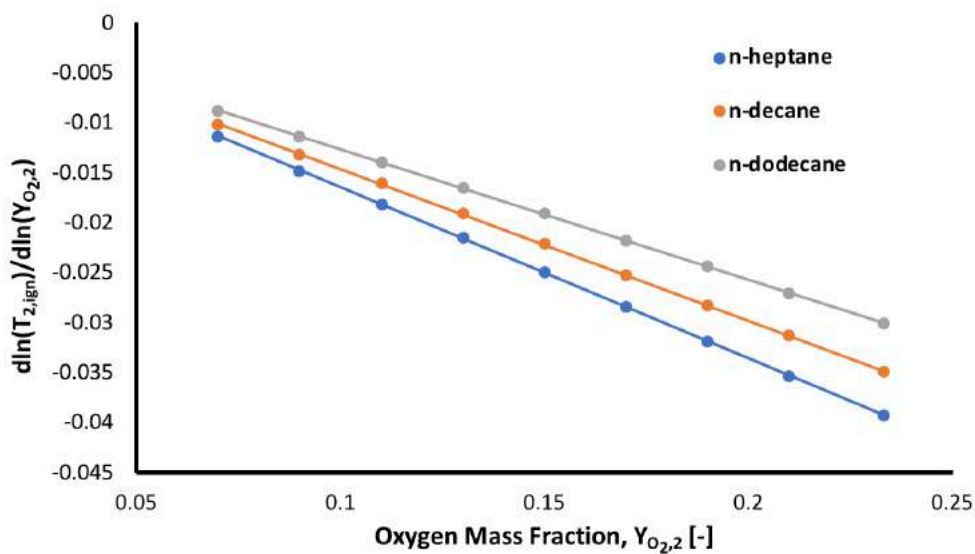
Figure 15 shows the fractional change in the values of the temperature at autoignition with fractional changes in the value of $Y_{O_2,2}$, $dlnT_{2,ign}/dlnY_{O_2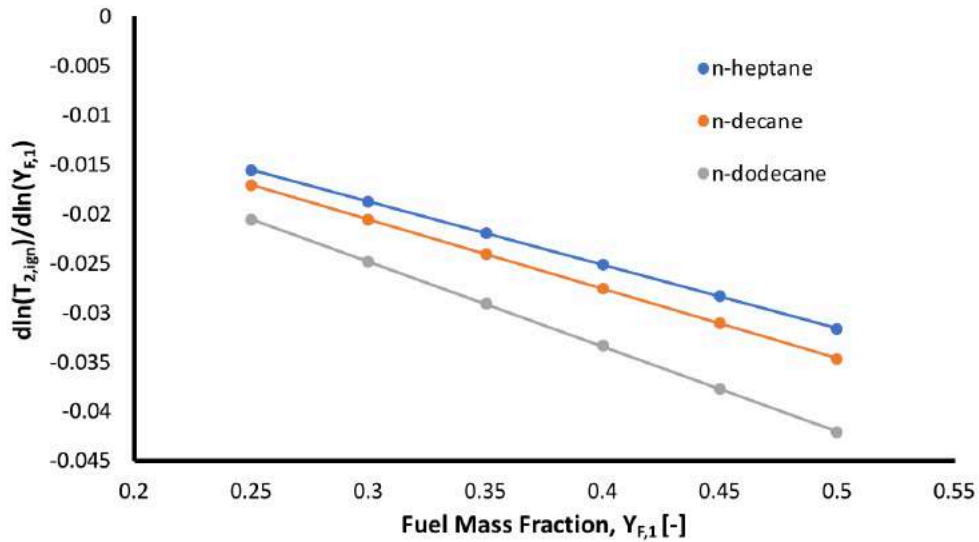,2}$, as a function of the oxygen mass fraction $Y_{O_2,2}$. This figure was constructed using the data shown in Figure 10. Figure 16 shows the fractional change in the values of the temperature at autoignition with fractional changes in the value of $Y_{F,1}$, $dlnT_{2,ign}/dlnY_{F,1}$, as a function of the oxygen mass fraction $Y_{F,1}$. This figure was constructed using the data shown in Figure 11. Both figures also indicate again that a variation of the fuel mass fraction has a greater influence on the autoignition temperature compared to a variation of the oxygen mass fraction. Of great interest is a comparison of the results from the counterflow experiments with results from the so-called shock tube experiments, where

the ignition delay time τ is measured. In such experiments the ignition delay time is correlated with the following formula [10]

$$\tau = A\left[exp\left(\frac{T_a}{T}\right)\right]\left(\frac{Y_F}{W_F}\right)^a\left(\frac{Y_{O_2}}{W_{O_2}}\right)^b W_{av}^{(a+b)}\left(\frac{p}{R}\right)^{(a+b)}\left(\frac{1}{T}\right)^{(a+b)}. \tag{4.1}$$

In this formula A is a constant, $Y_{F,1}$ is the fuel mass fraction, Y_{O_2} is the oxygen mass fraction, W_F is the molecular weight of fuel, W_{O_2} is the molecular weight of oxygen, W_{av} is the average molecular weight, p is the pressure, R is the gas constant, T the temperature, $a = 0.4$, $b = -1.20$, and $T_a = 20211.37\ [K]$.

This formula shows an increase in the autoignition temperature T assuming fixed τ and Y_{O_2} and a fixed fuel mass fraction Y_F. Whereas the results which were carried out in the counterflow setup show that with increasing Y_F, the autoignition temperature T decreases.

Figure 15: The fractional change in the values of the temperature at autoignition with fractional changes in the value of $Y_{O_2,2}$, $dlnT_{2,ign}/dlnY_{O_2,2}$, as a function of the oxygen mass fraction $Y_{O_2,2}$.

Figure 16: The fractional change in the values of the temperature at autoignition with fractional changes in the value of $Y_{F,1}$, $dlnT_{2,ign}/dlnY_{F,1}$, as a function of the oxygen mass fraction $Y_{F,1}$.

4.2. Results of the Extinction Experiments

The extinction experiments were carried out to investigate the influence of different fuel mass fractions Y_F on the critical conditions of extinction. The experiments with different fuel mass fractions were conducted from the lowest fuel mass fraction of $Y_{F,1} = 0.25$ to the highest fuel mass fraction of $Y_{F,1} = 0.5$. The displayed experimental data points are arithmetically averaged values.

Figure 17 shows the experimental results of different mass fraction of fuel, $Y_{F,1}$, as a function of the strain rate at extinction, a_2, for n-heptane, n-decane and n-dodecane. Furthermore, the results show that n-dodecane is easiest to extinguish followed by n-decane and n-heptane. This means that heavier hydrocarbons tend to extinguish easier before lighter hydrocarbons. All investigated fuels show the same trend.
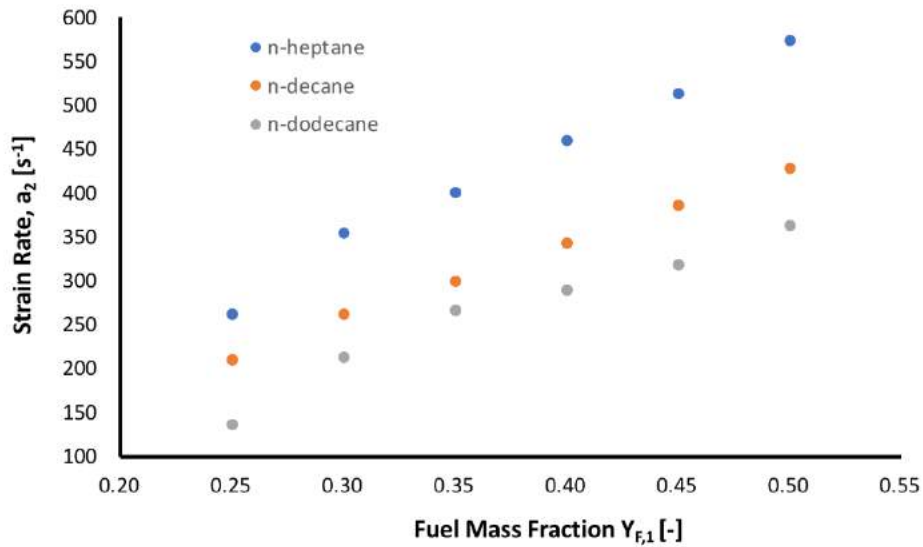
Figure 17: The extinction strain rate a_2 as a function of the mass fraction of fuel $Y_{F,1}$ for $T_1 = 533.15\ [K]$ and $Y_{O_2,2} = 0.233$.

The kinematic models for the extinction experiments were carried out with OpenSMOKE++ using two detailed chemical-kinematic mechanisms made up of more than 400 grid points among more than 100 species. For the numerical simulations plug flow conditions were used to describe the flow field and both Soret effect and gas radiation were included in the simulations. At the fuel-boundary and oxidizer-boundary, the temperatures, T_1 and T_2 and the injection speeds of the fuel-stream v_1, oxidizer-stream v_2, are prescribed.

The numerical extinction limits are compared in Figure 18 and Figure 19 with the reported experimental data. For the numerical calculations two different mechanism, the full and the skeletal mechanism, was used. The full mechanism includes high temperature chemistry and the skeletal mechanism includes both high and low temperature chemistry. It can be seen that the models predict the critical conditions fairly well over a wide range of different fuel mass fractions. The lines represent boundaries which separate a flammable from a nonflammable region.

In Figure 18 it can be seen that for n-heptane, the skeletal mechanism data agrees very well by the model with an average error of the same order of magnitude of the experimental uncertainty. The computational data of n-decane and n-dodecane over predict the data obtained from the experiments, but it still shows the same trend.
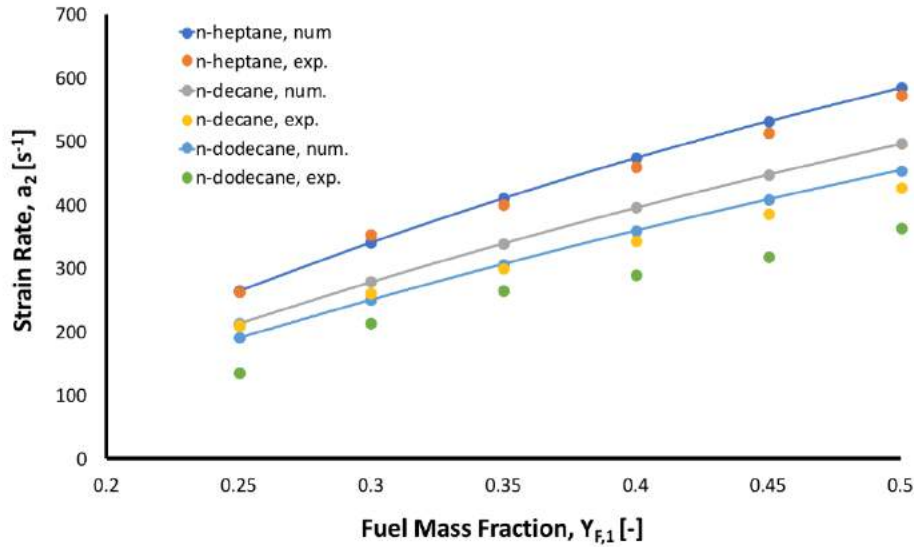
Figure 18: Comparison of the skeletal mechanism calculations with the experimental results of the extinction strain rate a_2 as a function of the mass fraction of fuel $Y_{F,1}$ for $T_1 = 533.15\ [K]$ and $Y_{O_2,2} = 0.233$.

Figure 19 shows that all 3 predictions improve when using a full mechanism. The average error drops from 2.7 % to 1.8 % for n-heptane, from 11.4 % to 7.0 % for n-decane and from 24.9 % to 18.1 % for n-dodecane.
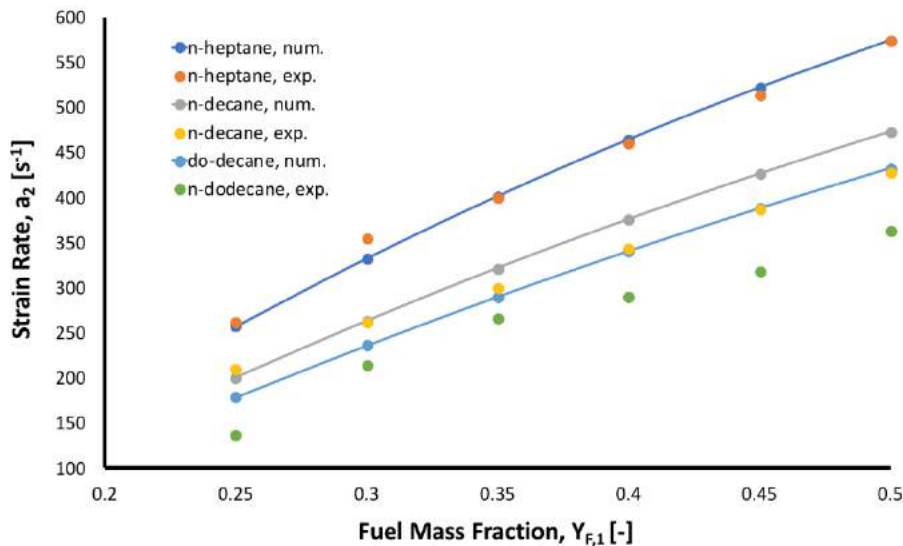
Figure 19: Comparison of the full mechanism calculations with the experimental results of the extinction strain rate a_2 as a function of the mass fraction of fuel $Y_{F,1}$ for $T_1 = 533.15\ [K]$ and $Y_{O_2,2} = 0.233$.

5. Autoignition of High Molecular Hydrocarbon Fuels at Elevated Pressures

The objective of the following chapter is to present numerical simulations of combustion processes in elevated pressure environments. The numerical results are used to study the combustion of high molecular weight hydrocarbon fuels in a counterflow burner with laminar nonuniform flows. Developing such an understanding is important to the further development of modern combustion devices to reduce pollution emissions and increasing the efficiency. The modern gasoline engines with direct injection and turbocharging have become a key technology in recent years. Modern gasoline direct injection systems achieve a savings potential of up to 15 percent in their fuel consumption and CO_2 emissions. These gasoline engines already have a high medium-pressure level and are characterized above all by a very high level of efficiency. To achieve even greater potential based on the downsizing strategy, future engines will achieve a significantly higher-pressure level. However, this increase in the pressure level in the gasoline combustion engine leads to undesirable combustion phenomena which can subsequently lead to engine damages and an increase in pollutant emissions. Many different combustion devices, such as aircraft engines, rocket engines and diesel engines, operate at pressure levels from 30 up to more than $100\ bar$. The influence of different fuel mass fractions $Y_{F,1}$ on autoignition at different elevated pressure levels are simulated and analyzed with the goal to help to develop advanced combustion control strategies and comprehensive understanding of combustion phenomena at elevated pressures.

5.1. Discussion of the Numerical Results of the Autoignition Event at Elevated Pressures

In Figure 17 the numerical results of the influence of different pressure levels on the temperature of the oxidizer stream at autoignition, $T_{2,ign}$, as a function of the mass fraction of fuel $Y_{F,1}$ for n-heptane are illustrated. The computational results show an increase of the autoignition temperature $T_{2,ign}$ by decreasing the fuel mass fraction. This is observed for all three different pressure levels and it shows the same characteristic as depicted in Figure 9, Figure 11 and Figure 13. It also can be seen that

the temperature of the oxidizer stream at autoignition $T_{2,ign}$ decreases as the pressure increases.
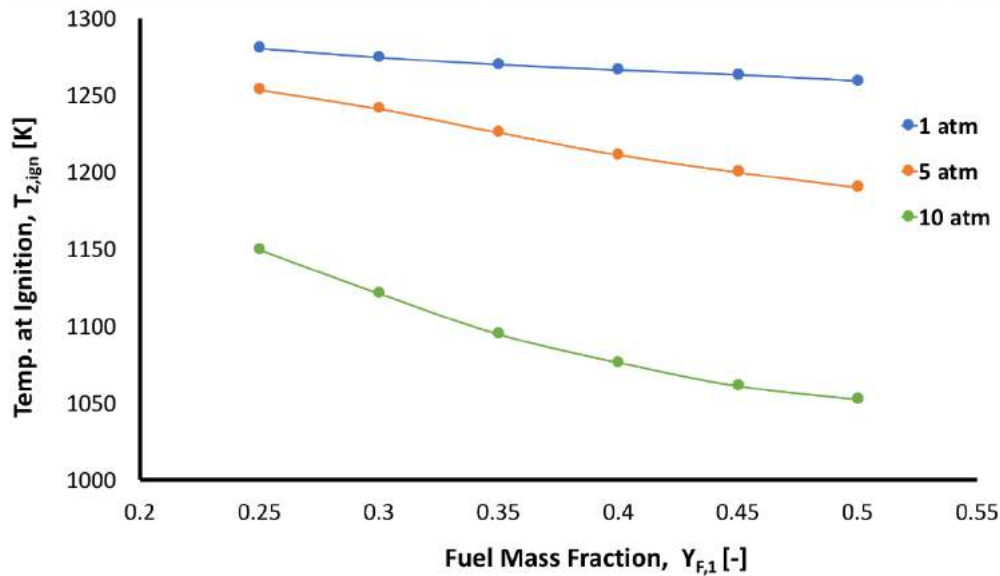
Figure 20: Numerical calculations of the temperature of the oxidizer stream at autoignition $T_{2,ign}$ at different pressure levels as a function of the mass fraction of fuel $Y_{F,1}$ for $Y_{O_2,2} = 0.233$, $T_1 = 533.15\ [K]$ and $a_2 = 550\ s^{-1}$.

6. Concluding Remarks

The main focus of this diploma thesis was aimed to help to understand the influence of reactants on critical conditions of autoignition and extinction of high molecular hydrocarbon fuels in nonpremixed, nonuniform flows. Furthermore, numerical simulations were carried out to show the influence of different pressure levels on the temperature of the oxidizer stream at autoignition as a function of the mass fraction of fuel as well as the mass fraction of oxygen.

The experimental studies of the critical conditions of autoignition show that the autoignition temperature increases with reducing the oxygen mass fraction. Furthermore, the autoignition characteristics of the tested fuels show a similar characteristic even at different fuel stream temperatures and it can also be shown that the autoignition temperature decreases by increasing the fuel stream temperature and of all testes fuels n-dodecane showed the highest autoignition temperature due to the highest number of hydrocarbons. Since the numerical simulations show almost no

influence on the oxygen content on the autoignition temperature, it is assumed that an error occurs in the low temperature mechanism and further improvement of the mechanism is necessary. The results also show that a variation of the fuel mass fraction has a greater influence on the autoignition temperature compared to a variation of the oxygen mass fraction, but they still show the same characteristic. The experimental results of the reference fuels were analyzed and found to be in general agreement with the predictions of kinetic models conducted by RECK Modeling Group of Politecnico di Milano. The computational results at different elevated pressures show an increase of the autoignition temperature $T_{2,ign}$ by decreasing the fuel mass fraction. This is observed for all three different pressure levels. It also can be seen that the temperature of the oxidizer stream at autoignition decreases as the pressure increases.

During the extinction experiments it was found that the extinction strain rate increases almost linear with increasing the fuel mass fraction. Two different numerical mechanisms were performed, and both match the experiments very well.

References

[1] G. P. Merker and C. Schwarz, Combustion Engines Development - Mixture Formation, Combustion, Emissions and Simulation, Berlin: Springer, ISBN: 978-3-642-02951-6, 2012.

[2] R. van Basshuysen,, Handbuch Verbrennungsmotor - Grundlagen, Komponenten, Systeme, Perspektiven, Berlin: Springer, ISBN: 978-3-658-04677-4, 2014.

[3] R. Seiser, K. Seshadri, E. Piskernik and A. Linan, Ignition in the Viscous Layer Between Counterflowing Streams - Asymptotic Theory with Comparison to Experiments, Department of Mechanical and Aerospace Engineering at University of California at San Diego, Departamento de Motopropulsión y Termofluidodinámica Universidad Politécnica de Madrid, 2000.

[4] J. Warnatz, U. Maas and R. W. Dibble, Combustion - Physical and Chemical Fundamentals, Modeling and Simulation, Experiments, Pollutant Formation, Berlin Heidelberg: Springer, ISBN: 978-3-540-25992-3, 2006.

[5] K. Seshadri and F. A. Williams, Laminar Flow between parallel Plates with Injection of a Reactant at high Reynolds Number, International Journal of Heat and Mass Transfer, 21(2):251–253, 1978.

[6] "NIST Chemistry WebBook, SRD 69," 2017. [Online]. Available: https://webbook.nist.gov/cgi/cbook.cgi?ID=142-82-5. [Accessed 01 01 2018].

[7] "NIST Chemistry WebBook, SRD 69," 2017. [Online]. Available: https://webbook.nist.gov/cgi/cbook.cgi?ID=124-18-5. [Accessed 01 01 2018].

[8] "NIST Chemistry WebBook, SRD 69," 2017. [Online]. Available: https://webbook.nist.gov/cgi/cbook.cgi?ID=C112403&Mask=200. [Accessed 01 01 2018].

[9] C. R. Shaddix, "Correcting Thermocouple Measurements for Radiation Loss - a critical Review," in *Proceedings of the 33rd National Heat Transfer Conference*, Livermore, 1999.

[10] M. B. Colket and L. J. Spadaccini, "Journal of Propulsion and Power, 17 (2001) 315–323.," *Journal of Propulsion and Power,* vol. 17, pp. 315-323, 2001.

[11] G. Dusan and D. Gruden, Umweltschutz in der Automobilindustrie - Motor, Kraftstoffe Recycling, Wießbaden: Vieweg+Teubner, ISBN: 978-3-8348-0404-4, 2008, 2008.

[12] G. Merker, C. Schwarz, G. Stiesch and F. Otto, Verbrennungsmotoren - Simulation der Verbrennung und Schadstoffbildung, Wiesbaden: Vieweg+Teubner Verlag, ISBN: 978-3-8351-9069-6, 2006.

[13] C. K. Law, Combustion Physics, Cambridge: Cambridge University Press, ISBN: 9780511754517, 2010.

[14] C. Mortimer, Chemie - Basiswissen der Chemie, Stuttgart: Thieme, ISBN: 3134843072, 2001, 2001.

[15] M. Kieberger, Untersuchung des Phänomens der Vorentflammung bei der ottomotorischen Verbrennung zur Bestimmung von Einflussfaktoren von Auslösemechanismen, Dissertation at Institute for Powertrains and Automotive Technology Vienna University of Technology, 2012.

[16] J. Jarosinski and B. Veyssiere, Combustion Phenomena - Selected Mechanism of Flame Propagation, and Extinction, Taylor & Francis Group, ISBN: 978-0-8493-8409-7, 2009.

[17] A. Linan, The asymptotic structure of counterflow diffusion flames for large activation energies, Acta Astronautica, 1(7-8):1007–1039, 1974.

[18] F. E. Fendell, Ignition and extinction in combustion of initially unmixed reactants, Journal of Fluid Mechanics, 21(2):291–303, 1965.

[19] K. A. Connors, Chemical Kinetics - The Study of Reaction Rates in Solution, New York: John Wiley & Sons, ISBN: 978-0471720201, 1990.

[20] B. R. Bird, W. E. Stewart and E. N. Lightfoot, Transport Phenomena, New York: John Wiley & Sons, ISBN: 0-471-41077-2, 2002.

[21] U. Niemann, K. Seshadri and F. A. Williams, "sciencedirect," 09 December 2014. [Online]. Available: https://ac.els-cdn.com/S0010218014003757/1-s2.0-S0010218014003757-main.pdf?_tid=50611f7a-e907-4c41-97eb-9cebdd13304a&acdnat=1523656973_403d566e9410265bb082e16b2603b2a3. [Accessed 13 April 2018].

[22] R. Gehmlich, Experimental Studies on Nonpremixed Combustion at Atmospheric and Elevated Pressures, Dissertation, University of California, San Diego, 2015.

[23] "Neutrium," 24 August 2012. [Online]. Available: https://neutrium.net/properties/properties-of-air/. [Accessed 07 February 2018].

[24] "Thermopedia," 2011 February 2011. [Online]. Available: http://www.thermopedia.com/fr/content/553/. [Accessed 07 February 2018].

[25] I. L. Roberts, J. E. Coney and B. M. Gibbs, "schiencedirect," 12 March 2012. [Online]. Available: https://ac.els-cdn.com/S1359431111001529/1-s2.0-S1359431111001529-main.pdf?_tid=9aec1925-1237-44f3-8e9a-63453d177daf&acdnat=1524529470_b746e9b20c24c0167b73589deab7d131. [Accessed 23 April 2018].

Figures